

Communication

A Compact Super-Wideband High Bandwidth Dimension Ratio Octagon-Structured Monopole Antenna for Future-Generation Wireless Applications

Naineri Suguna  and Senthil Revathi *

School of Electronics Engineering, Vellore Institute of Technology, Vellore 632014, India; reachsuguna@gmail.com

* Correspondence: srevathi@vit.ac.in

Abstract: A high-dimension ratio, octagonal-shaped, super-wideband (SWB) monopole antenna was proposed in this paper. The proposed antenna was composed of an octagonal-structured radiating patch with a flower-shaped slot fed by a linearly tapering microstrip line and a rectangular partial ground fabricated on a Rogers 5880 dielectric substrate, with an overall dimension of $14 \times 16 \times 0.787 \text{ mm}^3$. The designed antenna exhibits SWB characteristics over the frequency range of 3.71 to 337.88 GHz at $|S_{11}| \leq -10 \text{ dB}$, $VSWR < 2$, a bandwidth ratio (BR) of 91.07:1, and a very high BDR of 6057.27. The proposed SWB antenna was designed, simulated, and analyzed using Ansys high-frequency structural simulator (HFSS). The simulated and measured findings have good confirmability, making them ideal for future-generation mobile networks, due to their strong radiation properties, compactness, and extremely wide bandwidth.

Keywords: polygon structure; tapered feed; super-wideband (SWB); bandwidth dimension ratio (BDR); peak gain; radiation efficiency



Citation: Suguna, N.; Revathi, S. A Compact Super-Wideband High Bandwidth Dimension Ratio Octagon-Structured Monopole Antenna for Future-Generation Wireless Applications. *Appl. Sci.* **2023**, *13*, 5057. <https://doi.org/10.3390/app13085057>

Academic Editor: Jaume Anguera

Received: 12 March 2023

Revised: 5 April 2023

Accepted: 5 April 2023

Published: 18 April 2023



Copyright: © 2023 by the authors. Licensee MDPI, Basel, Switzerland. This article is an open access article distributed under the terms and conditions of the Creative Commons Attribution (CC BY) license (<https://creativecommons.org/licenses/by/4.0/>).

1. Introduction

In the digital era, there is a massive demand for ultra-fast data transmission, and audio and video transmission with minimal latency in modern wireless technologies. In addition, in today's "everything and everyone is connected" world, the use of smart devices is increasing at an exponential rate, necessitating extremely wide bandwidth, compact antennas with strong radiation properties, and multiband functionality capable of supporting both short- and long-range transmission [1,2]. The Federal Communications Commission (FCC) assigned unlicensed frequency ranges of 3.1 to 10.6 GHz to ultra-wideband (UWB) technology in 2002 [3,4]. Over the past two decades, the potentials of high data rate, simplicity, low cost, low noise, high accuracy, and low power spectral density have attracted a great deal of attention. An antenna operating with a ratio bandwidth of 3.4:1 is called a UWB antenna, which enables short-range, high-speed data transmission between electronic devices. However, an antenna with a ratio bandwidth (RBW) equal to or greater than 10:1 at $|S_{11}| \leq -10 \text{ dB}$ over the entire frequency range of interest is called an SWB antenna. Rumsey et al. initially developed frequency-independent SWB antennas in the late 1950s and early 1960s. These antennas consist of equiangular spiral and log-periodic structures [5]. Unlike UWB antennas, SWB antennas do not have any predefined operating frequency band standards. SWB antennas are extremely compact, have a broad bandwidth over any frequency range of the electromagnetic spectrum, and support both short- and long-range transmission. In designing SWB antennas, it is not sufficient to evaluate the antenna performance in traditional parameters such as gain and radiation patterns, etc. To verify the capability of the antenna to operate as a SWB antenna, the bandwidth dimension ratio (BDR) is introduced as an index term to determine both the compactness and wideband characteristics of an antenna. It is necessary to maintain a consistent group delay of < 2 nano seconds for the entire band as well. The

monopole antenna is a promising SWB antenna due to its compact dimensions, inexpensive, linear design, incredibly high BW impedance, and simplicity of integration into handheld devices [6–8].

Many wideband antennas were reported in the literature for SWB applications, such as a concentric Mickey-Mouse-shaped monopole radiator with a semi-elliptical ground for super-wideband (SWB) application, which was presented with an electrical size of $0.16 \lambda \times 0.18 \lambda$ (λ lowest cutoff frequency). The antenna operates over the frequency range of 1.22–47.5 GHz and offers an FBW of 190% and a RBW of 38.9:1 with a peak gain of 0.5 to 10.3 dBi [9]. A medically designed pill-shaped microstrip patch antenna [10] with a physical size of $41 \times 32 \times 16 \text{ mm}^3$ was designed to achieve a peak gain of 8.2 dBi and operates over 2–95 GHz with BDR 3095, FBW 180%, and a low efficiency of 67%. A novel monopole antenna with a partial ground plane in the shape of a trapezoid and patches in the shape of semicircles with a tapered feed line was designed to achieve a high bandwidth dimension ratio (BDR) of 4261.007. An antenna operates in the frequency range of 1.30 to 20 GHz with an impedance bandwidth of 175.58%, a low ratio bandwidth of 15.38:1, and a low average peak gain of 4.18 dBi [11]. A compact SWB antenna was designed on a flexible Ultralam 3850 laminate substrate for 5G and IOT applications with dimensions of $60 \times 40 \times 0.1 \text{ mm}^3$ and operates in the frequency band from 1.74 to 100 GHz with a 57.47:1 ratio bandwidth (BW). A peak gain of 9.24 dB at 65.6 GHz and even lower than 0 dB of gain was observed in the designed band [12]. A circularly shaped asymmetrical dipole antenna with two dielectric substrates of low permittivity was designed with a 21.9:1 ratio bandwidth and $VSWR < 2$ [13]. A triple elliptical monopole antenna with overall dimensions of $27 \text{ mm} \times 29.5 \text{ mm}$ was fabricated on a Roger's RT-Duroid 5880 substrate with a relative permittivity of (ϵ_r) = 2.2 and a loss tangent of ($\tan \delta$) = 0.0009 and covers the frequency band from 1.91 to 43.5 GHz at $S_{11} \leq -10 \text{ dB}$ with a very BDR of 5761.87, a FBW > 183.17%, and a RBW of 22.77:1 [14]. A wide band scarecrow-shaped ultra-wide band (UWB) antenna using CPW and microstrip line-feeding technique was reported with a dimension of $5 \times 20 \times 1.6 \text{ mm}^3$. The IBW of a CPW-fed antenna and a microstrip-line-fed antenna was 2.51–16.48 GHz (147.13%) and 2.86–16.17 GHz (139.88%), respectively [15]. A trapezoid-shaped monopole radiator fed by a triangular, tapered feed line and a semicircular ground was presented. The electrical size was $0.16 \lambda_c \times 0.27 \lambda_c$ and offered a SWB range of 1.42–90 GHz at $S_{11} \leq -10 \text{ dB}$, a bandwidth ratio of 63.30:1, and a $VSWR \leq 2$ [16]. A psi-shaped circularly polarized antenna with high gain and bandwidth was investigated and found to be best suited for detection of the blind spots of a vehicle in V2V and V2R communications [17]. An elliptical-shaped fractal antenna in a tree-structured configuration for super-wideband applications was proposed. The antenna has a size of $170 \times 150 \text{ mm}^2$ and provides an IBW of 0.65 to 35.61 GHz, a ratio bandwidth of 54.78:1, a peak realized gain of 6.51 dB, and an average gain of 3.24 dB [18].

An octagonal, ring-shaped, $40 \times 40 \times 1.01 \text{ mm}^3$ sized monopole antenna with a stub placed on the top of the right corner was developed to enhance the impedance bandwidth over a range of 2.59 to 31.14 GHz at $|S_{11}| \leq -10 \text{ dB}$ [19]. A triple-notch super-wideband antenna with a bandwidth of 2.34 GHz to 20 GHz was designed and fabricated for Bluetooth and LTE 2600 bands, and achieved a gain of 4.98 dBi and radiation efficiency of 89% [20]. An offset elliptical ring patch antenna with a tapered feed line was developed. The proposed antenna has a ratio bandwidth of 34.63:1, a bandwidth dimension ratio of 1732, and a peak gain of 5.81 dBi over the functional frequency range of 2.31–40.0 GHz [21]. A compact bulb-model planar super-wideband SWB antenna was designed with the dimensions of $35 \times 30 \times 0.8 \text{ mm}^3$ and works in the frequency range of 2.8–40 GHz with a RBW of 14.28:1. The antenna has a FBW of 173.8% and a BDR of 1904. A FSS was placed on top of the radiating patch with an air gap of 19 mm to enhance gain over the specified SWB range [22]. A Sierpinski fractal antenna was designed with a patch in the shape of a hexagon and coplanar waveguide feeding. The bandwidth ratio of 11:1 was achieved over an impedance bandwidth of 3.4–37.4 GHz [23]. A star-triangular fractal monopole antenna feed with microstrip-fed and semielliptical ground plane was investigated with

a footprint of $20\text{ mm} \times 20\text{ mm} \times 1\text{ mm}^3$ and exhibited a super-wideband range of 1–30 GHz with $\text{VSWR} < 2$ [24]. The SWB antennas reported in [9–24] have limited FBW, BDR, and radiation performance. Therefore, the major issues in the design of SWB antennas are miniaturization, wide impedance bandwidth, and a high BDR.

A compact super-wideband antenna was presented and analyzed in this article. It consists of an octagonal radiating patch fed by a linearly tapered microstrip line and the partial ground plane. The proposed antenna achieved a super-wideband frequency range of 3.71–337.88 GHz, a fractional bandwidth of 195.65%, and a very high bandwidth dimension ratio of 6057.27, with an overall size of $14\text{ mm} \times 16\text{ mm}$. VSWR, efficiency, and radiation patterns were also investigated to support SWB applications.

2. Antenna Design Methodology

The geometrical parameters of the patch antenna are computed using conventional mathematical formulas [25,26], and then applied to area of an octagon to derive its dimensions. An octagonal patch antenna is constructed on the basis of a circular patch antenna. The area of the octagonal and circular geometry is nearly equal, as shown in Figure 1. The dimensions of the circular and octagonal shapes are determined using Equations (1)–(4) and optimized for the better antenna performance.

$$\pi a_e^2 = 2(1 + \sqrt{2})s^2 \tag{1}$$

where ‘ a_e ’ is effective radius of circular patch due to fringing effect

$$a_e = a \left[1 + \frac{2h}{\pi a \epsilon_r} \left\{ \ln \left(\frac{\pi a}{2h} \right) + 1.7726 \right\} \right]^{1/2} \tag{2}$$

‘ a ’ is the actual radius of the circular patch and is derived as

$$a = \frac{F}{1 + \frac{2h}{\pi F \epsilon_r} \left[\ln \left(\frac{\pi F}{2h} \right) + 1.7726 \right]^{1/2}} \tag{3}$$

where

$$F = \frac{8.791 * 10^9}{f_r \sqrt{\epsilon_r}} \tag{4}$$

The proposed monopole antenna with various evaluations are shown in Figure 2. The electrical dimension of the antenna is $0.16 \lambda_c \times 0.18 \lambda_c$, where the wavelength λ_c is the lowest operating frequency or physical size of $14\text{ mm} \times 16\text{ mm}$. It is printed on Rogers RT/Duroid 5880TM dielectric substrate with a permittivity (ϵ_r) of 2.2 and a height (h) of 0.787 mm. The physical dimensions of substrate are $W_s \times L_s$, where $W_s = 14\text{ mm}$ and $L_s = 16\text{ mm}$. The presented antenna has an octagonal-shaped radiating patch, tapered feed microstrip line, and partial ground plane. To achieve optimal matching, the width of the feed line is reduced linearly from $W_2 = 2\text{ mm}$ to $W_1 = 1.5\text{ mm}$, while the length of the feed line $L_f = 6.3\text{ mm}$ remains constant. The ground plane length $L_g = 6\text{ mm}$, and the radius of the circle patch (R) = 4.5 mm, from which the octagonal sides are derived. The edge of the octagon, $S = 3.45\text{ mm}$, and the elliptical slots D1, D2, D3, and D4 are used in the patch to construct a flower-shaped slot in the octagonal radiating patch. A very wide frequency range is also dependent on the geometry of the ground, and the time of the current path determines the lowest cut off frequency. As a result, rectangular ground becomes a partially ground plane.

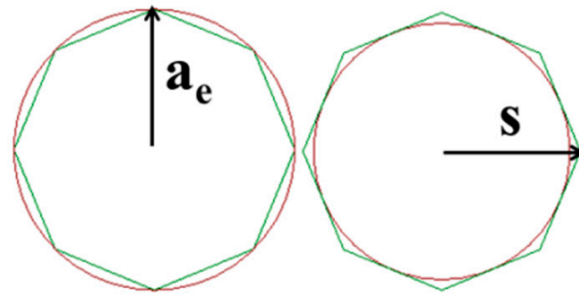


Figure 1. Area correlation between circular and octagon geometry.

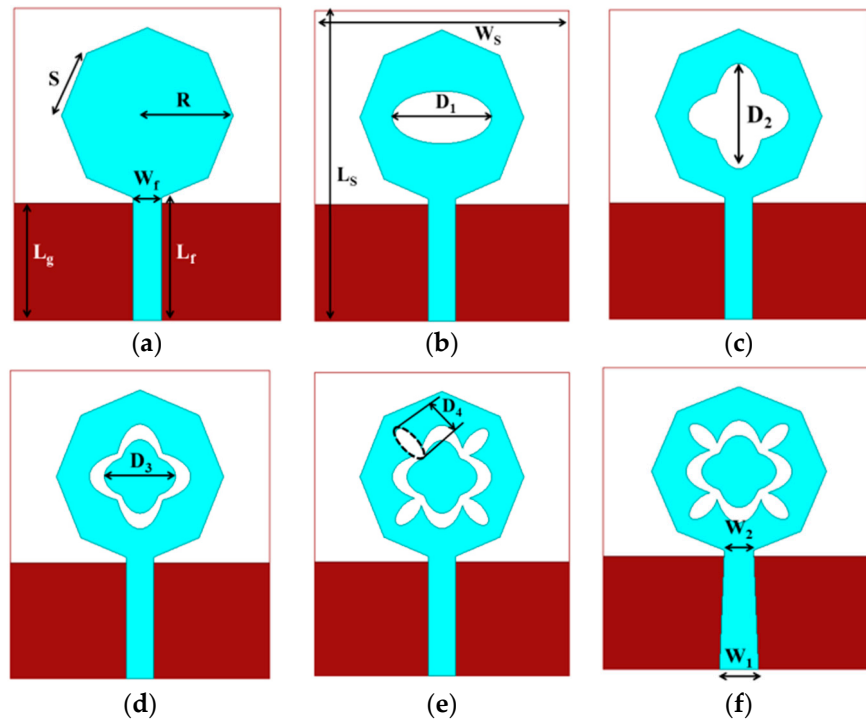


Figure 2. Geometry of SWB antenna with different design evaluations (a) iteration 1, (b) iteration 2, (c) iteration 3, (d) iteration 4, (e) iteration 5, (f) iteration 6.

Evaluations of SWB Monopole Antenna Configuration

Different evaluations of the octagonal structured proposed monopole antenna with a partial ground plane are shown in Figure 2. The octagonal radiating patch designed on Rogers RT/Duroid 5880™ material with partial ground geometry is shown in Figure 2a. An elliptical aperture is cut into the octagon patch to enhance its impedance bandwidth, as shown in Figure 2b. The Babinet principle is applied during this process. The elliptical slot is converted into a plus-shaped elliptical slot and embedded into the patch, as shown in Figure 2c. When the self-similar modified plus structure is merged with the preceding geometry, a new ring-slotted octagon patch is formed, as shown in Figure 2d. The octagonal structure that is carved into the flower-shaped slot is shown in Figure 2e. Furthermore, IBW and BDR are improved by switching from a rectangular 50 Ω transmission feed line to a tapered feed line, as shown in Figure 2f. The dimensions of the evaluated geometries are listed in Table 1.

Table 1. Novel self-similar slotted monopole antenna with partial ground plane dimensions given in mm.

Design Parameters	Dimensions	Design Parameters	Dimensions
L_f	6.3	D_1	5.45
W_f	1.5	D_2	5.45
L_g	6	D_3	3.8
S	3.45	D_4	1.8
R	4.5	W_1	1.5
L_s	16	W_2	2
W_s	14		

3. Results and Discussion

3.1. Electromagnetic Characteristics

The proposed super-wideband monopole antenna is analyzed in terms of reflection coefficient (S11), voltage standing-wave ratio (VSWR), and input impedance (Z_{in}), as shown in Figures 3–5.

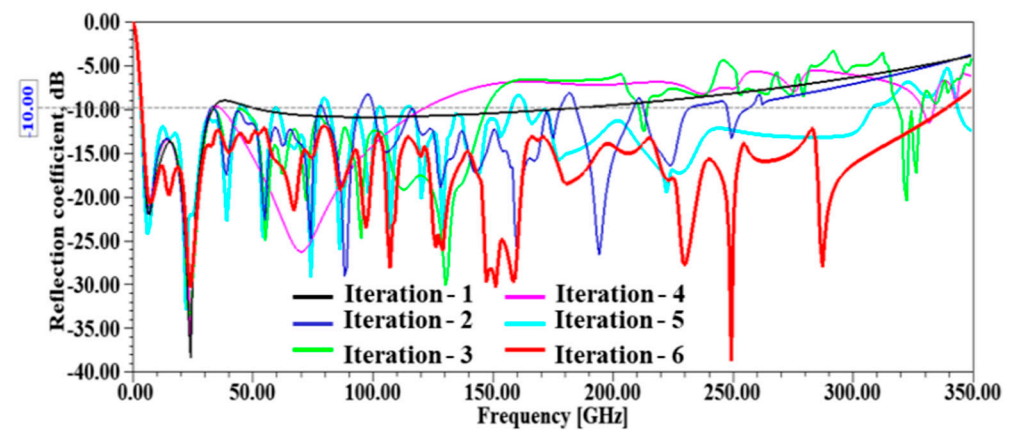


Figure 3. Simulated reflection – coefficient of proposed antenna.

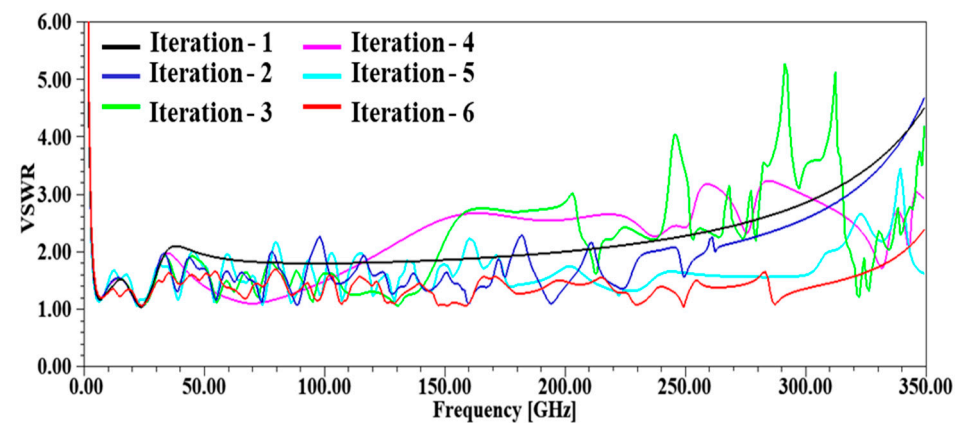


Figure 4. VSWR of the proposed antenna.

Figure 3 demonstrates the reflection coefficient of the proposed antenna for all the iterations from 1 to 6, whose electrical characteristics are summarized in Table 2. In iteration 1, an eight-sided polygon radiating element of the copper conductor layer with a partial ground plane is developed, and this antenna has a maximum reflection coefficient (S11) of -38.41 dB at resonance frequency of 24.1 GHz and an impedance bandwidth (IBW) of 29.69 GHz over a frequency range of 3.49 – 33.18 GHz with $S_{11} \leq -10$ dB, as shown in Figure 3. In iteration 2, an elliptical slot is etched into the polygon structure to obtain wider bandwidth characteristics, while the ground plane remains unchanged from the first

step. As shown in Figure 3, this antenna covers multiple bands in the desired spectrum, and the corresponding IBWs are 28.67 GHz, 42.73 GHz, 14.82 GHz, 15.56 GHz, 61.1 GHz, 23.58 GHz, and 18.52 GHz, as listed in Table 2. The antenna design has been modified to avoid notches by incorporating an elliptical plus-shaped slot into the octagonal patch design. Iteration 3, provides bandwidths of 3.54–33.69 GHz and 45.28–147.10 GHz, with respective FBWs of 161.96% and 105.85%. There is a significant enhancement in both the wide and fractional bandwidths, though the notches are not completely eliminated, as shown in Figure 3. In iteration 4, a plus-shaped ring is etched into a conventional octagon, which enhances the fractional bandwidth and bandwidth characteristics illustrated in Figure 3. These characteristics restrict the fractional bandwidth of two broad bands to 161.36% and 105.76%, respectively. In iteration 5, the radiating element is optimized by integrating the minor elliptical slots and the ring slots to resemble a flower structure. The bandwidth is increased to cover the frequency range of 3.37 GHz to 307.24 GHz with minor notch bands at 43.80–47.15 GHz, 58.82–60.47 GHz, 77.98–81.87 GHz, 101.92–103.88 GHz, 113.03–116.49 GHz, and 157.39–171.96 GHz with the modified structure. In addition to the notch bands, the iterative structure exhibits a huge bandwidth, which covers a wide range of wireless applications. The main objective of the proposed structure is to cover a wide band spectrum suitable for a diverse range of wireless applications such as industrial, scientific, and medical (ISM), radar, satellite, navigation, sensing, explosive detection, short-range indoor applications, etc. Iteration 6 transforms a 50 Ω transmission line into a tapered-fed structure with a partial ground plane. The proposed monopole structure with optimized geometry, as shown in Figure 3, has an operating range of 3.71–337.88 GHz at $S_{11} \leq -10$ dB and an impedance bandwidth of 334.17 GHz, a bandwidth ratio (BR) of 91.07, and a fractional bandwidth (FBW) of 195.65%, as stated in Table 2. The proposed antenna achieves a very high bandwidth dimension ratio (BDR) of 6057.27 due to the novel structure. The simulated VSWR graph of design evaluations from conventional polygons to proposed geometry is shown in Figure 4. A low VSWR across the operating band indicates low mismatch losses, low reflected power, and effective impedance matching. The mathematical relation between mismatch loss (ML) and VSWR is shown in Equation (5).

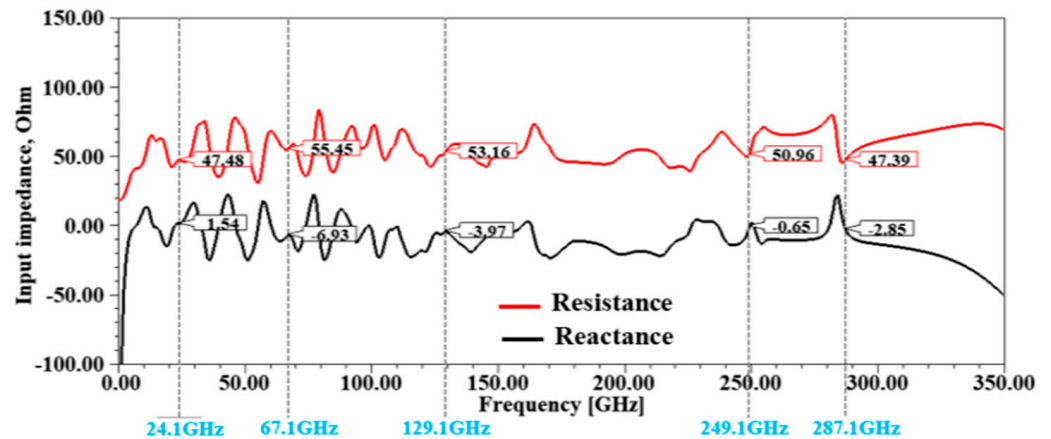


Figure 5. Simulated input impedance of designed antenna: real and imaginary part.

$$ML = -10 \log \left[1 - \left[\frac{VSWR - 1}{VSWR + 1} \right]^2 \right] \tag{5}$$

Table 2. Electrical characteristics summary of designed antenna in various stages.

S. No	Design	Operating Bandwidth, GHz	Impedance Bandwidth, GHz	Bandwidth Ratio, BR	Fractional Bandwidth, FBW %	VSWR
1	Iteration 1	3.49–33.18	29.69	9.507	161.93%	1.03
		3.43–32.10	28.67	9.35	161.38%	1.06
		34.32–77.05	42.73	2.24	76.73%	1.14
		79.37–94.19	14.82	1.18	17.07%	1.08
2	Iteration 2	100.27–115.83	15.56	1.15	14.40%	1.44
		116.65–177.75	61.1	1.52	41.50%	1.09
		184.63–208.21	23.58	1.12	12.00%	1.09
		212.68–231.20	18.52	1.08	8.34%	1.35
3	Iteration 3	3.54–33.69	30.15	9.51	161.96%	1.04
		45.28–147.10	101.82	3.24	105.85%	1.06
4	Iteration 4	3.54–33.11	29.57	9.35	161.36%	1.02
		37.17–120.58	83.41	3.24	105.75%	1.10
		3.37–43.80	40.43	12.99	171.42%	1.04
		47.15–58.82	11.67	1.24	22.08%	1.11
5	Iteration 5	60.47–77.98	17.51	1.29	25.29%	1.07
		81.87–101.92	20.05	1.24	21.81%	1.23
		103.88–113.03	9.15	1.08	8.43%	1.13
		116.49–157.39	40.9	1.35	29.86%	1.13
6	Iteration 6	171.96–307.24	135.28	1.78	56.46%	1.23
		3.71–337.88	334.17	91.07	195.65%	1.02

The significant enhancements in operating bandwidth, impedance bandwidth, bandwidth ratio, fractional bandwidth, and VSWR for each antenna iteration are shown in Table 2. The values are computed using Equations (6), (7), (8), and (9), respectively.

Impedance bandwidth (IBW):

$$IBW = f_h - f_l \quad (6)$$

Bandwidth ratio (BR):

$$BR = f_h / f_l \quad (7)$$

Fractional bandwidth (FBW):

$$FBW = \frac{2 * (f_h - f_l)}{(f_h + f_l)} * 100 \quad (8)$$

where f_l is the low cut-off frequency, and f_h is the high cut-off frequency, and VSWR of iterations 1–6.

BDR is an essential parameter in SWB antennas because it implies the antenna compactness and wider bandwidth. BDR denotes the proportion of bandwidth that an antenna can provide per unit electrical area. BDR is defined mathematically [5] as Equation (9).

$$BDR = \frac{Bandwidth \%}{\lambda_{length} \times \lambda_{width}} \quad (9)$$

where λ is the lowest cutoff frequency of operating spectrum.

The input impedance (Z_{in}) characteristics of the proposed tapered-fed monopole element with a partial ground plane are shown in Figure 5. At resonant frequencies of 24.1 GHz, 67.1 GHz, 129.1 GHz, 249.1 GHz, and 28 GHz, the resistance (R_{in}) and reactance (X_{in}) values are $47.48 + j1.54 \Omega$, $55.45 - j6.93 \Omega$, $53.16 - j3.97 \Omega$, $50.96 - j0.65 \Omega$, and $47.39 - j2.85 \Omega$, respectively, and are listed in Table 3.

Table 3. Input impedance of proposed antenna at selected resonant frequencies.

S. No	Resonant Frequency	Resistance, R_{in}	Reactance, X_{in}	Input Impedance, Z_{in}
1	24.1 GHz	47.48 Ω	1.54 Ω	47.48 + j1.54 Ω
2	67.1 GHz	55.45 Ω	-6.93 Ω	55.45 - j6.93 Ω
3	129.1 GHz	53.16 Ω	-3.97 Ω	53.16 - j3.97 Ω
4	249.1 GHz	50.96 Ω	-0.65 Ω	50.96 - j0.65 Ω
5	287.1 GHz	47.39 Ω	-2.85 Ω	47.39 - j2.85 Ω

3.2. Radiation Characteristics

The proposed antenna is simulated using the Ansys HFSS simulator tool, which produces peak gains of 2.31 dBi at 24.1 GHz, 6.11 dBi at 67.1 GHz, 12.00 dBi at 129.1 GHz, 14.14 dBi at 249.1 GHz, and 14.29 dBi at 287.1 GHz, as shown in 3D gain polar plots in Figure 6. Also, 2D far-field patterns in E-plane and H-plane are shown in Figure 7. At low frequencies, the current is distributed uniformly across the ground plane and patch (Figure 6a,b). As a result, radiation patterns in the E and H planes are omnidirectional. At mid- and higher frequencies, higher-order modes are generated, and the current density on the radiator is not as evenly distributed. Therefore, the radiated modes are more prone to high radiation interference or minor lobes. As illustrated in Figure 6c–e, deterioration in the omnidirectional nature of the radiation pattern begins with an increase in frequency. Various techniques, such as periodic structures, defected ground structures (DGS), parasitic elements, and split ring resonators, can be employed to suppress these undesired radiated modes, thereby improving the performance of the proposed antenna over the SWB range.

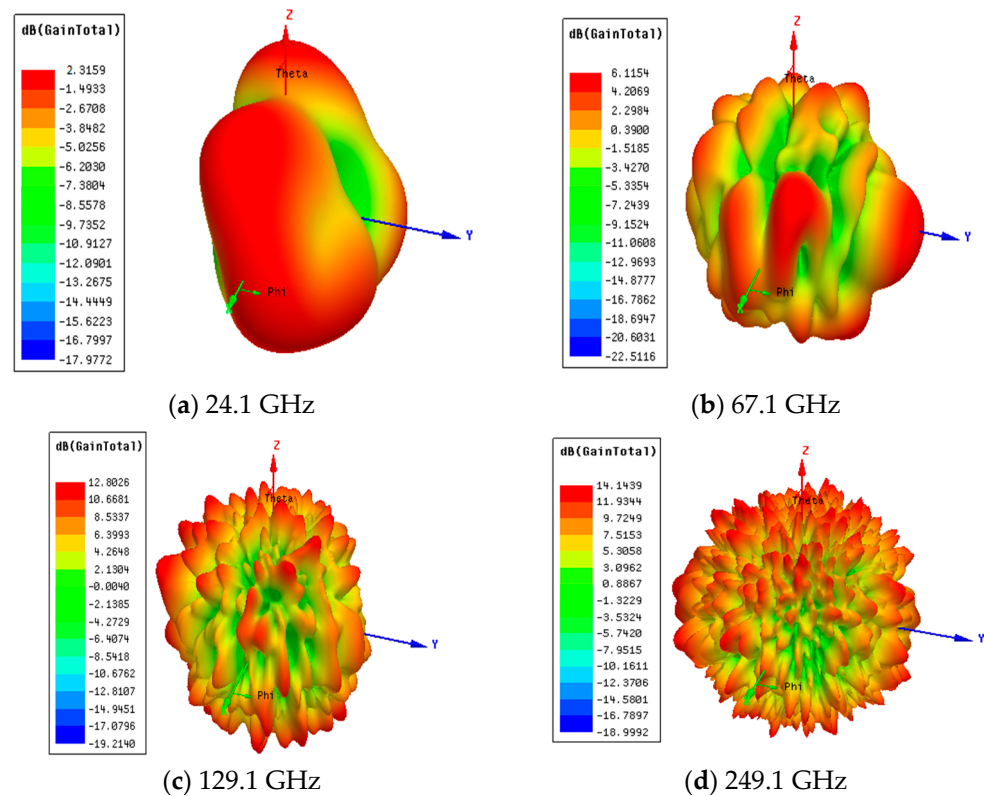
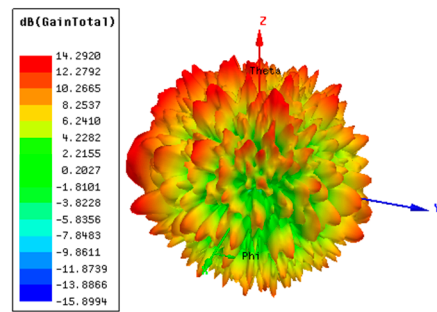


Figure 6. Cont.



(e) 287.1 GHz

Figure 6. The 3D gain polar plots of the final iterative design of the proposed tapered-fed structure with partial ground plane.

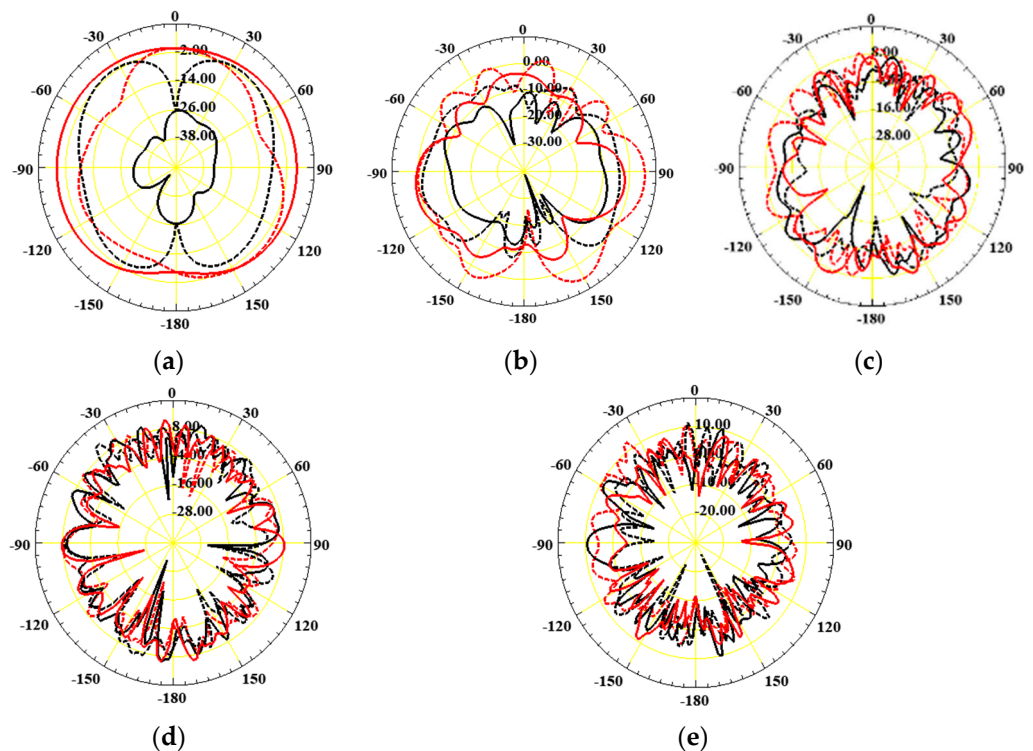


Figure 7. The 2D far-field patterns in E-plane and H-plane: (a) 24.1 GHz, (b) 67.1 GHz, (c) 129.1 GHz, (d) 249.1 GHz, (e) 287.1 GHz (red solid—co-polarized E-plane; black solid—cross-polarized E-plane; red dotted line—co-polarized H-plane; black dotted line—cross-polarized H-plane).

3.3. Surface Current Analysis

The performance of a super-wideband (SWB) antenna is analyzed using surface current dissipation, as shown in Figure 8a–e. Current is more concentrated around the feedline region and the edges of the minor elliptical slots, at the resonance frequencies of 24.1 GHz, 67.1 GHz, 129.1 GHz, 249.1 GHz, and 287.1 GHz of the final iteration of the proposed antenna, as shown in Figure 8a. Current flows through the feedline and concentrates at the slot edges depending on the phase angle, as shown in Figure 8b. The magnitude of the current at the feedline is higher at 129.1 GHz, as shown in Figure 8c. At higher resonant frequencies of 249.1 GHz and 287.1 GHz, more current flows to the feed line and ground plane, as shown in Figure 8d,e. The iterations in the antenna design produce a fringing field, which improves the coupling mechanism between the radiating layers. As a result, the impedance of the proposed monopole antenna increases.

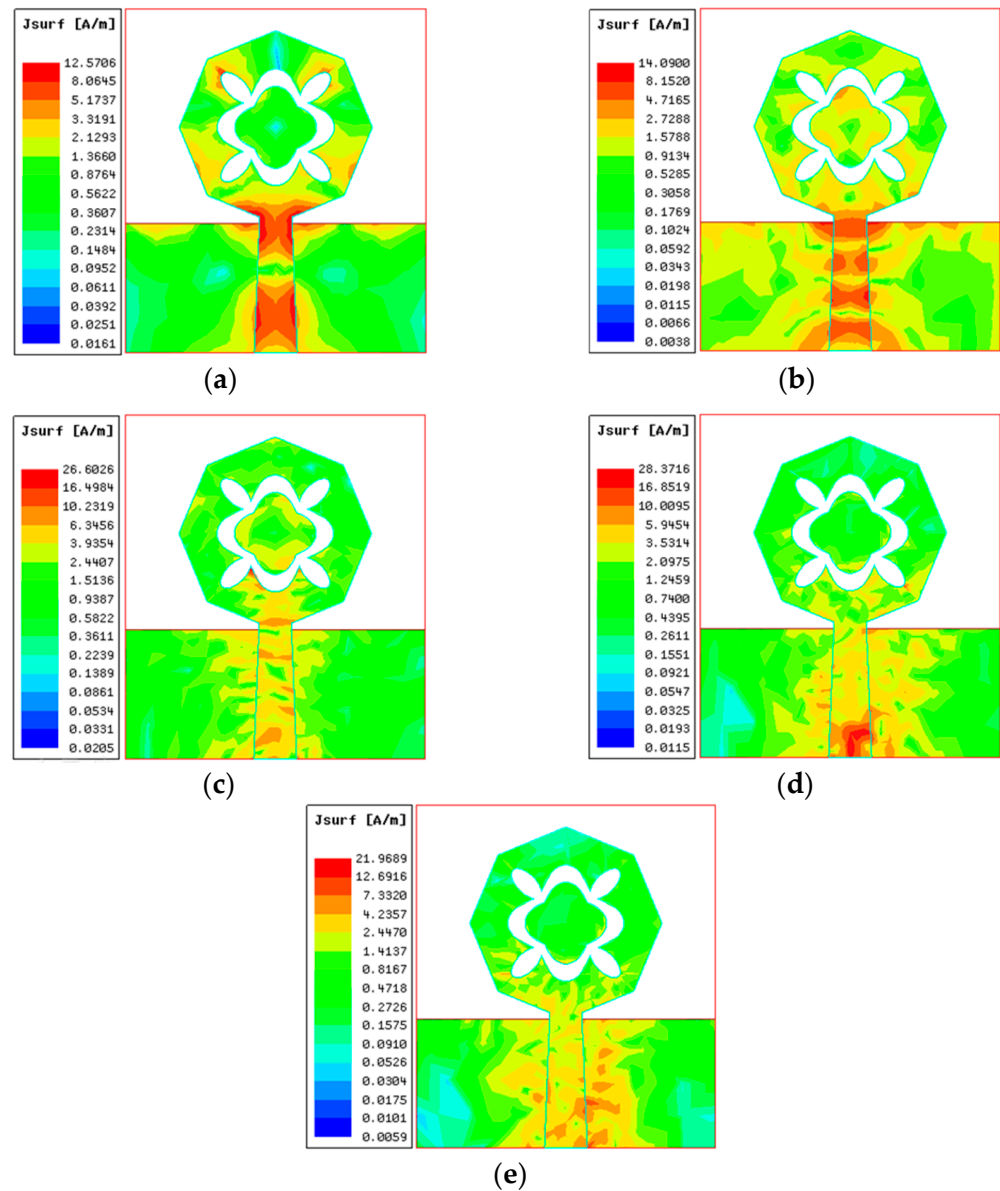


Figure 8. The surface current distribution of the designed antenna for (a) 24.1 GHz, (b) 67.1 GHz, (c) 129.1 GHz, (d) 249.1 GHz, (e) 287.1 GHz.

3.4. Gain and Radiation Efficiency Characteristics

The simulated gain (G) and radiation efficiency (η) of a SWB monopole antenna are shown in Figures 9 and 10. The proposed design has a peak-realized gain of 18.01 dB and a radiation efficiency of 62–95% in the super-wideband frequency range of 3.71–337.88 GHz. As shown in Figure 9, there is a minor discrepancy between realized gain and total gain up to 255.56 GHz, and an exponential drop at higher operating frequencies due to mismatch losses and reflection losses at the input port. Similarly, as shown in Figure 10, these losses affect the radiation efficiency in the same manner. This high gain is achieved by etching a flower-shaped slot into a radiator and employing a partial ground and tapered feed technique.

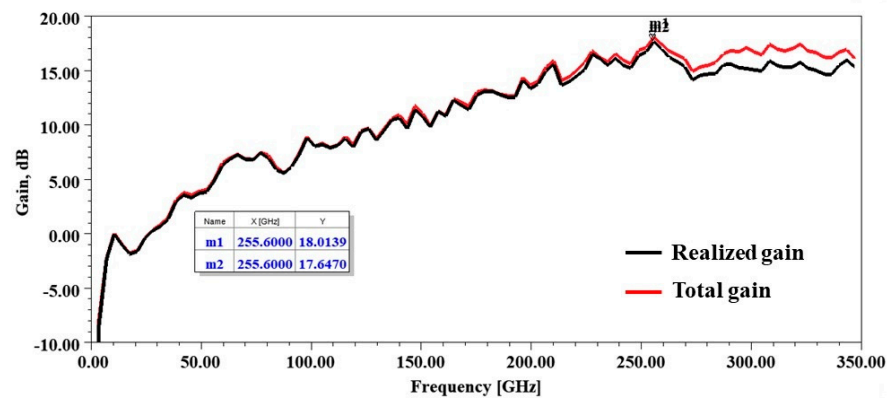


Figure 9. Gain-characteristics of the suggested antenna.

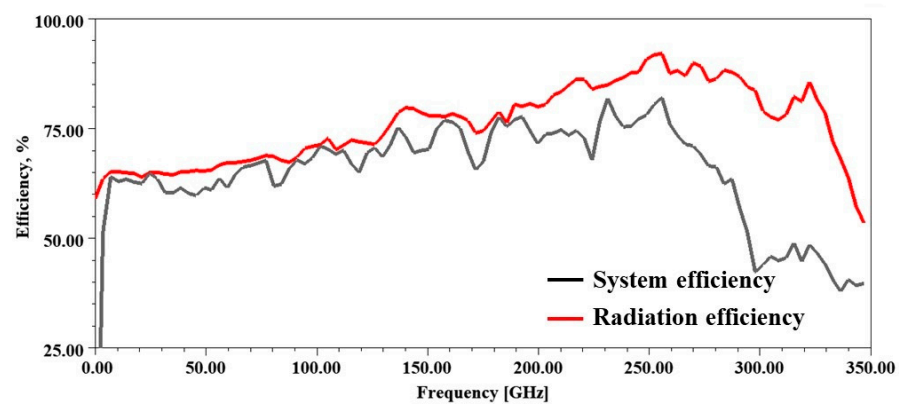


Figure 10. Efficiency characteristics of the suggested antenna.

3.5. Fabricated Prototype and Measured Results

The front and rear views of the fabricated prototypes of a proposed monopole SWB antenna printed using a DMP-2800 Dimatix Fujifilm conductive material printer on Rogers RT/Duroid 5880TM material are displayed in Figure 11. The simulated and measured reflection coefficients, VSWR properties, and their enlarged views are shown in Figures 12 and 13, respectively. The performance of fabricated antennas is measured using an Agilent E5071B vector network analyzer (VNA), and Figures 12 and 13 demonstrate a strong similarity between the simulation and the experimental outcomes.

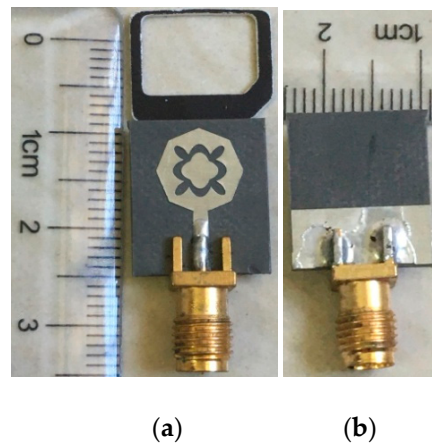


Figure 11. Fabricated prototype: (a) front view, (b) rear view.

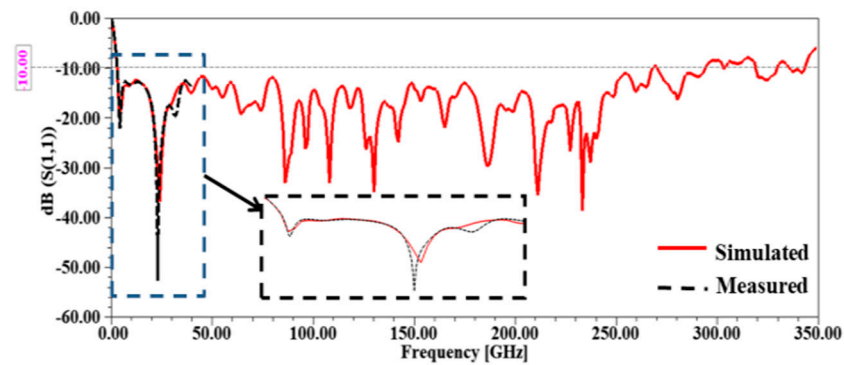


Figure 12. Simulated and measured return loss of the proposed SWB monopole antenna.

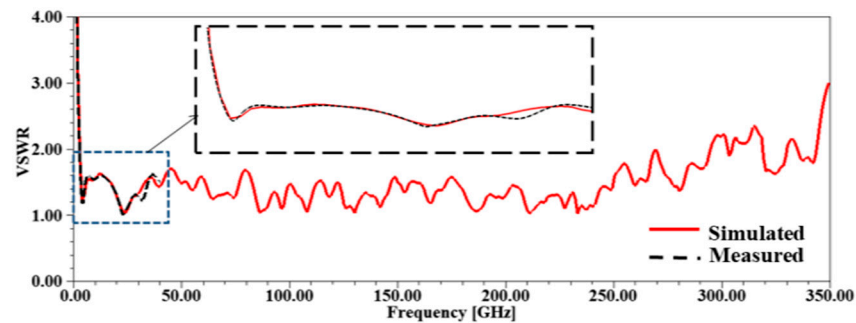


Figure 13. Simulated and measured VSWR of the proposed SWB monopole antenna.

4. Comparison of Proposed Monopole SWB Antenna with Reported Works

The performance comparison of the proposed design and a few recently reported SWB antenna designs [9–24] is shown in Table 4. The proposed antenna exhibits high gain characteristics, excellent SWB response with very high dimension ratio, and a compact size.

Table 4. Comparison to the reported SWB antenna structures.

Ref.	PS, mm ²	E.S, λ _o ²	f _l , GHz	f _h , GHz	IBW, GHz	FBW, %	BR	BDR	S ₁₁ , dB	G, dB	η, %
Tiwari et al. [15]	25 × 20	0.20 × 0.16	2.51	16.48	13.97	147.13	6.57	4597.81	−20	5.5	NR
Mondal et al. [17]	58.2 × 47.7	0.97 × 0.8	5	7	2	33.33	1.40	43.23	−22.5	NR	NR
Rahman et al. [16]	57 × 34	0.26 × 0.16	1.42	90	88.58	193.70	63.38	4483.79	−41	7.67	98.9
Singhal et al. [18]	170 × 150	0.37 × 0.33	0.65	35.61	34.96	192.83	54.78	1610.83	NR	6.51	NR
Okan et al. [19]	40 × 40	0.35 × 0.35	2.59	31.14	28.55	169.29	12.02	1419.52	−39	2–5	90–99
Dhasarathan et al. [20]	28 × 20	0.21 × 0.15	2.34	20	17.66	158.10	8.55	5019.11	−20	5.25	NR
Sharma et al. [21]	39 × 39	0.3 × 0.3	2.31	40	37.69	178.16	17.32	1975.62	−40	5.81	NR
Ayyappan et al. [14]	27 × 29.5	0.17 × 0.187	1.91	43.5	41.59	188.51	22.77	5761.87	−62	8.15	90.08
This Work	14 × 16	0.16 × 0.18	3.71	337.88	334.17	195.65%	91.07	6057.27	−38.77	18.01	62–95

Notation: PS—physical size, E.S—electrical size, fl—flower resonant frequency, fh—higher resonant frequency, IBW—impedance bandwidth, FBW—fractional bandwidth, BR—bandwidth ratio, BDR—bandwidth dimension ratio, S₁₁—reflection coefficient, G—peak gain, η—radiation efficiency, NR—not reported.

5. Conclusions

A novel portable super-wideband monopole antenna with an octagonal structure was designed for diverse wireless communication applications. The proposed antenna was developed using an octagonal-shaped radiator with microstrip line-feeding. The radiation and bandwidth properties of the antenna were analyzed, and the results demonstrate its suitability for wideband applications. SWB antennas, unlike UWB antennas, are not limited to 3.1–10.6 GHz. Hence, the suggested SWB antenna was compared to reported antenna structures in the literature in terms of physical dimensions, electrical dimensions, impedance bandwidth, bandwidth ratio, bandwidth dimension ratio, fractional bandwidth, VSWR, reflection loss, gain, and efficiency. It is found that a compact SWB antenna is realized and exhibits a very wide bandwidth, a high BDR of 6057.27, and a high realized gain (G) of 18.01 dB with a miniaturized volume. A prototype was developed and measured

with the help of the agile vector network analyzer. Even though the proposed antenna operates effectively over the super-wideband frequency spectrum of 3.71–337.88 GHz with a $|S_{11}| \leq -10$ dB, the experimental results are measured only up to 40 GHz due to the higher frequency limitation of the available VNA. The benefits of proposed makes it useful for S, C, X, Ku, K, Ka, V, and W mm wave bands, future-generation mobile networks (i.e., 5G and beyond (B5G)), military and civilian applications, cognitive radios for spectrum sensing, radio astronomy for space exploration, satellite communications, and amateur radio for terrestrial and planetary communications.

Author Contributions: Conceptualization: N.S. and S.R.; methodology, N.S. and S.R.; software, N.S.; validation, N.S. and S.R.; formal analysis, N.S. and S.R.; investigation, N.S. and S.R.; resources, N.S.; data curation, N.S. and S.R.; writing—original draft preparation, N.S.; writing—review and editing, S.R.; visualization, N.S. and S.R.; supervision, S.R. All authors have read and agreed to the published version of the manuscript.

Funding: This research received no external funding.

Institutional Review Board Statement: Not applicable.

Informed Consent Statement: Not applicable.

Data Availability Statement: Not applicable.

Conflicts of Interest: The authors declare no conflict of interest.

References

1. Khan, F.; Pi, Z. mmWave mobile broadband (MMB): Unleashing the 3–300GHz spectrum. In Proceedings of the 34th IEEE Sarnoff Symposium, Princeton, NJ, USA, 16 June 2011; pp. 1–6.
2. Rappaport, T.S.; Xing, Y.; MacCartney, G.R.; Molisch, A.F.; Mellios, E.; Zhang, J. Overview of millimeter wave communications for fifth-generation (5G) wireless networks—With a focus on propagation models. *IEEE Trans. Antennas Propag.* **2017**, *65*, 6213–6230. [[CrossRef](#)]
3. FCC. *First Report and Order in the Matter of Revision of Part 15 of the Commission's Rules Regarding Ultra-Wideband Transmission Systems*; FCC: Washington, DC, USA, 2002; pp. 98–153. ISSN 1937-8718.
4. Wiesbeck, W.; Adamiuk, G.; Sturm, C. Basic properties and design principles of UWB antennas. *Proc. IEEE* **2009**, *97*, 372–385. [[CrossRef](#)]
5. Rumsey, V. Frequency independent antennas. In Proceedings of the 1958 IRE International Convention Record, New York, NY, USA, 20–23 August 1957; pp. 114–118.
6. Balani, W.; Sarvagya, M.; Ali, T.; Pai, M.M.; Anguera, J.; Andujar, A.; Das, S. Design techniques of super-wideband Antenna—Existing and future prospective. *IEEE Access* **2019**, *7*, 141241–141257. [[CrossRef](#)]
7. Ali, T.; Subhash, B.K.; Pathan, S.; Biradar, R.C. A compact decagonal-shaped UWB monopole planar antenna with truncated ground plane. *Microw. Opt. Technol. Lett.* **2018**, *60*, 2937–2944. [[CrossRef](#)]
8. Chen, K.R.; Row, J.S. A compact monopole antenna for super wideband applications. *IEEE Antennas Wirel. Propag. Lett.* **2011**, *10*, 488–491. [[CrossRef](#)]
9. Balani, W.; Sarvagya, M.; Samasgikar, A.; Ali, T.; Kumar, P. Design and analysis of super wideband antenna for microwave applications. *Sensors* **2021**, *21*, 477. [[CrossRef](#)]
10. Maity, S.; Tewary, T.; Mukherjee, S.; Roy, A.; Sarkar, P.P.; Bhunia, S. Super wideband high gain hybrid microstrip patch antenna. *AEU-Int. J. Electron. Commun.* **2022**, *153*, 154264. [[CrossRef](#)]
11. Samsuzzaman, M.; Islam, M.T. A semicircular shaped super wideband patch antenna with high bandwidth dimension ratio. *Microw. Opt. Technol. Lett.* **2015**, *57*, 445–452. [[CrossRef](#)]
12. Dey, S.; Arefin, M.S.; Karmakar, N.C. Design and experimental analysis of a novel compact and flexible super wide band antenna for 5G. *IEEE Access* **2021**, *9*, 46698–46708. [[CrossRef](#)]
13. Barbarino, S.; Consoli, F. Study on super-wideband planar asymmetrical dipole antennas of circular shape. *IEEE Trans. Antennas Propag.* **2010**, *58*, 4074–4078. [[CrossRef](#)]
14. Ayyappan, M.; Patel, P. On design of a triple elliptical super wideband antenna for 5G applications. *IEEE Access* **2022**, *10*, 76031–76043. [[CrossRef](#)]
15. Tiwari, R.N.; Singh, P.; Kanaujia, B.K. Small-size scarecrow-shaped CPW and microstrip-line-fed UWB antennas. *J. Comput. Electron.* **2018**, *17*, 1047–1055. [[CrossRef](#)]
16. Rahman, S.U.; Cao, Q.; Ullah, H.; Khalil, H. Compact design of trapezoid shape monopole antenna for SWB application. *Microw. Opt. Technol. Lett.* **2019**, *61*, 1931–1937. [[CrossRef](#)]

17. Mondal, T.; Maity, S.; Ghatak, R.; Bhadra Chaudhuri, S.R. Design and analysis of a wideband circularly polarised perturbed psi-shaped antenna. *IET Microw. Antennas Propag.* **2018**, *12*, 1582–1586. [[CrossRef](#)]
18. Singhal, S.; Singh, A.K. Elliptical monopole based super wideband fractal antenna. *Microw. Opt. Technol. Lett.* **2020**, *62*, 1324–1328. [[CrossRef](#)]
19. Okan, T. A compact octagonal-ring monopole antenna for super wideband applications. *Microw. Opt. Technol. Lett.* **2020**, *62*, 1237–1244. [[CrossRef](#)]
20. Dhasarathan, V.; Sharma, M.; Kapil, M.; Vashist, P.C.; Patel, S.K.; Nguyen, T.K. Integrated bluetooth/LTE2600 superwideband monopole antenna with triple notched (WiMAX/WLAN/DSS) band characteristics for UWB/X/Ku band wireless network applications. *Wirel. Netw.* **2020**, *26*, 2845–2855. [[CrossRef](#)]
21. Sharma, V.; Deegwal, J.K.; Mathur, D. Super-wideband compact offset elliptical ring patch antenna for 5G applications. *Wirel. Pers. Commun.* **2022**, *122*, 1655–1670. [[CrossRef](#)]
22. Kundu, S.; Chatterjee, A. A compact super wideband antenna with stable and improved radiation using super wideband frequency selective surface. *AEU-Int. J. Electron. Commun.* **2022**, *150*, 154200. [[CrossRef](#)]
23. Singhal, S.; Singh, A.K. CPW-fed hexagonal Sierpinski super wideband fractal antenna. *IET Microw. Antennas Propag.* **2016**, *10*, 1701–1707. [[CrossRef](#)]
24. Waladi, V.; Mohammadi, N.; Zehforoosh, Y.; Habashi, A.; Nourinia, J. A novel modified star-triangular fractal (MSTF) monopole antenna for super-wideband applications. *IEEE Antennas Wirel. Propag. Lett.* **2013**, *12*, 651–654. [[CrossRef](#)]
25. Mythili, P.; Das, A. Simple approach to determine resonant frequencies of microstrip antennas. *IEE Proc.-Microw. Antennas Propag.* **1998**, *145*, 159–162. [[CrossRef](#)]
26. Ray, K.P.; Kumar, G. Determination of the resonant frequency of microstrip antennas. *Microw. Opt. Technol. Lett.* **1999**, *23*, 114–117. [[CrossRef](#)]

Disclaimer/Publisher’s Note: The statements, opinions and data contained in all publications are solely those of the individual author(s) and contributor(s) and not of MDPI and/or the editor(s). MDPI and/or the editor(s) disclaim responsibility for any injury to people or property resulting from any ideas, methods, instructions or products referred to in the content.